Characterization of engine inlet flows by optical measurements of velocity profiles with high measurement rate

Andreas Fischer[1,*], Jörg König[1], Lars Büttner[1], Jürgen Czarske[1], Guido Stockhausen[2,*], Chris Willert[2]

1: Laboratory for Measuring and Testing techniques, Technische Universität Dresden, 01062 Dresden, Germany
2: Institute of Propulsion Technology, German Aerospace Center (DLR), 51170 Köln, Germany
*correspondent authors: andreas.fischer2@tu-dresden.de, guido.stockhausen@dlr.de

Abstract   For characterizing inlet flows of aircraft engines, grids of 40 pressure probes are applied as state-of-the-art for measuring the pressure fluctuations in the inlet with a typical measurement rate of 4 kHz. In order to get a more flexible and non-intrusive measurement setup, frequency modulated Doppler global velocimetry (FM-DGV) is applied in an inlet flow experiment for the first time measuring the flow velocity fluctuations. The novel approach includes using an imaging fiber bundle and an endoscope for light detection from inside the inlet without disturbing the flow significantly. The key challenge was to achieve a sufficiently high measurement rate, which is limited by the signal to noise ratio. In the experiment, measurement rates of up to 8 kHz were achieved. This proves the principle applicability of FM-DGV for inlet flow characterization. The single component setup consisted of 16 measurement points linearly aligned at a radial line (compared to 10 points with a probe rake). The measured mean velocity profiles were validated by the air mass flow rate. Measurements with 0.5 kg/s and 1 kg/s were accomplished. The resolved velocity spectra indicate significant flow oscillations up to about 1 kHz. As expected, the spectra show stronger oscillations when inserting a distortion plate. Hence, FM-DGV is proven to be a promising technique for the non-intrusive characterization of inlet flows at high measurement rates.

1. Introduction

Motivation of the measurement task
For aircraft engines, the incoming flow has to be both spatially and temporally uniform in order to ensure a stable engine operation at all flight conditions within the flight envelope [1]. For this reason, all turbine engines have an inlet section to homogenize the incoming flow. The inlet section has to be designed in such a way that the remaining inlet flow distortions can be tolerated by the engine. Otherwise a loss of the engine performance might result and the risk of an unstable engine operation increases. As a result, the inlet flow has to be characterized by means of measurements.

State-of-the-art and problem description
For this purpose, an aerodynamic interface plane (AIP) is defined, which represents the flow interface plane between inlet and engine [1]. The characterization of the inlet flow at the AIP is crucial to check if it meets the engine demands. The non-uniformity of the flow in the AIP is, among others, evaluated by measuring both the swirl as well as the total pressure distribution. Currently, this is accomplished with arrays of usually 40 five-hole probes or pressure probes, which are arranged along four radial lines [1,2]. Along one radial line, 10 probes are used. Typically the probe bandwidth has to be $\geq$ 4 kHz to capture the dynamic pressure. While this measurement procedure is an industrial standard (see "SAE ARP1420") [2] it has several disadvantages:

- intrusiveness of the probes,
- low number of measurement points,
- low flexibility and, thus, time-consuming and high costs, because one probe mesh cannot be used for different inlet models with different diameters.

General aim and solution approach
Non-intrusive optical measurement techniques on the other hand hold the potential of alleviating

some of the shortcomings of the probe measurement techniques and at the same time can further improve AIP characterization by providing data rates beyond 4 kHz. This would directly yield information on swirl distribution while the dynamic pressure can be derived from the velocity fluctuations. Adding dynamic pressure with the additionally measured static pressure finally yields the required total pressure distribution.

The key challenge besides multiple-point capability and a high measurement rate is to develop and/or apply a measurement technique that can cope with the limited optical access in the inlet. Here, Doppler global velocimetry (DGV) is presented as an appropriate measurement technique. DGV allows to measure three component velocity fields and easy imaging through fiber bundles because of its robustness against optical aberrations [3,4]. Using a fiber bundle is a flexible and simple solution for light detection from inside the inlet [5,6]. For observing large areas with an imaging fiber bundle, DGV is advantageous, because seeding particles do not have to be resolved in contrast to e. g. particle image velocimetry [7]. However, conventional DGV systems have typical measurement rates of a few Hertz maximum, which is not sufficient. For this reason, the recently developed frequency modulated DGV system [8,9] capable of maximum 100 kHz measurement rate is applied to an imaging fiber bundle to measure an engine inlet flow for the first time.

Aim and structure of the paper
In the paper, the setup of a frequency modulated Doppler global velocimeter (FM-DGV) and its first application to measure the flow velocity in the AIP of an inlet model is described. In the experiment, high measurement rates up to 8 kHz were achieved. The paper structure is as follows: In section 2, the FM-DGV measurement principle is briefly summarized. Subsequently, the setup of the experiment (inlet model) and the necessary modifications of the measurement system are described in section 3. Next, the measurement results are presented and discussed in section 4. The discussion of the results of this proof-of-principle experiment revealed promising prospects and options for future improvements, which are given in section 5. Finally, the most important findings are summarized in section 6.

2. FM-DGV measurement principle

FM-DGV measures the flow velocity $\vec{v}$ simultaneously at multiple points. The principle measurement arrangement for a single-component measurement is depicted in Fig. 1a: The flow region of interest is illuminated with a narrow band laser, whose frequency is modulated in time around a fixed center frequency. The laser light is scattered on particles, which were added to the flow and which are assumed to follow the flow with negligible slip. According to the Doppler effect, the center light frequency of the scattered light is shifted by [10]

$$f_D = f_c \frac{\left|\vec{o} - \vec{i}\right|}{c} \cdot v \qquad \text{with} \qquad v = \frac{(\vec{o} - \vec{i})}{\left|\vec{o} - \vec{i}\right|} \cdot \vec{v} \qquad (1)$$

and f_c as laser center frequency, $\vec{i}$ as laser incidence direction, $\vec{o}$ as observation direction and c as light velocity. Hence, the velocity component v along the vector ($\vec{o}$ - $\vec{i}$) is measured when evaluating the Doppler frequency f_D. The measurement of all three velocity components is possible for example by using two additional incidence angles of the laser. Further details about simultaneous measurements of multiple components with FM-DGV are beyond the scope of this paper and can be found in [11].

In order to measure the Doppler frequency of the scattered light, the laser is stabilized to the frequency of a molecular resonance and the Doppler shifted scattered light is observed through a molecular absorption cell with equal molecular resonance. The transmitted light is detected with a detector array allowing multiple point measurements. As is illustrated in Fig. 1b, the detector signals contain harmonics resulting from the sinusoidal laser frequency modulation and the non-

linear spectral transmission curve of the absorption cell. From the time series $s[n]$, $n = 0,..., N-1$, of each detector signal, the amplitude ratio

$$q = A_1 / A_2. \tag{2}$$

of the first and second order harmonic is evaluated, which depends on the Doppler frequency [9].
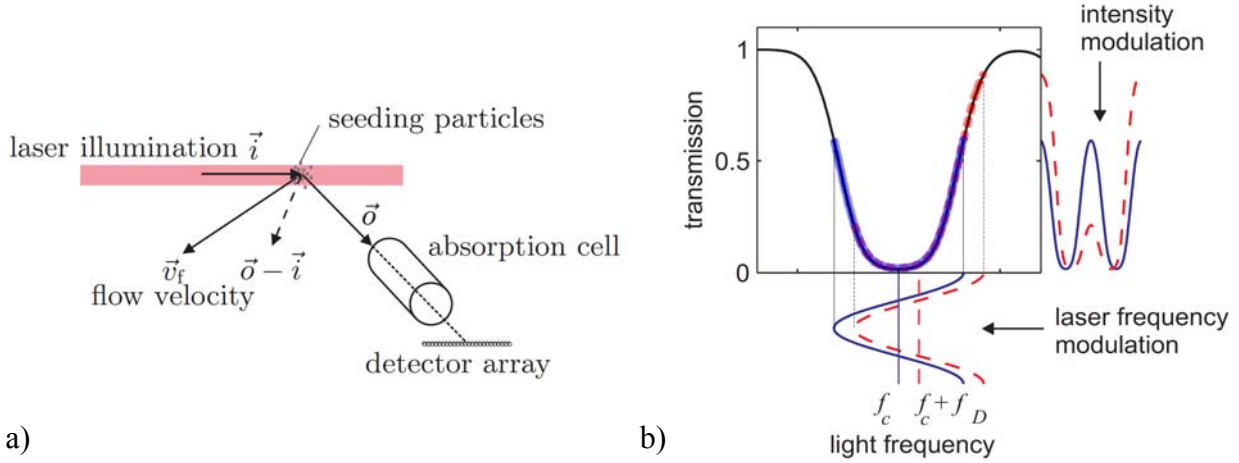

Fig. 1 a) Schematic set-up of the FM-DGV technique and b) transmission curve of the absorption cell and illustration of a typical sinusoidal laser frequency modulation (one modulation period)
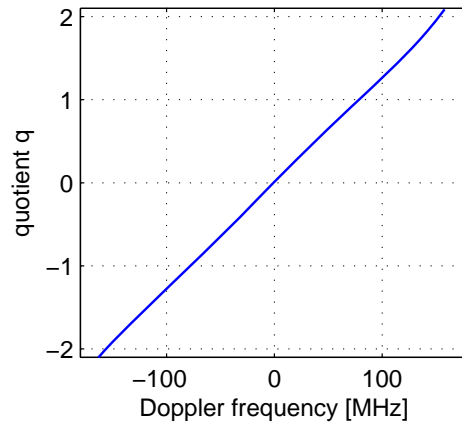

Fig. 2 Measured calibration curve of the FM-DGV measurement system

The amplitudes A_1, A_2 of the two harmonics are calculated according to the calculation of a Fourier coefficient by

$$A_k = \frac{2}{N} \sum_{n=0}^{N-1} s(n/f_a) \cdot \cos(2\pi k n f_m / f_a + \varphi_k), \qquad k = 1,2, \tag{3}$$

with f_m as modulation frequency, f_a as sampling frequency and φ_1, φ_2 as constant phases with respect to the sinusoidal laser frequency modulation. The phases are determined once e. g. by maximizing the amplitude results. In order to eliminate errors of the amplitude estimation due to leakage effects, only integer multiples of the modulation period are evaluated by choosing the corresponding number of samples. Hence, the estimation according to Eq. (3) produces the correct amplitude values without the need for a peak-detection algorithm.

The relation between q and f_D is usually obtained from a calibration measurement at a rotating disc with given rotation frequency. Thereby, the measured Doppler frequency can be converted into the velocity component v, and vice versa, with Eq. (1) according to the known measurement

arrangement and the known laser wavelength $\lambda = c \,/\, f_c$. The resulting curve of such a calibration measurement is shown in Fig. 2 as an example. For instance, the given measurement range $\pm$ 125 MHz of the Doppler frequency corresponds to a velocity measurement range of $\pm$ 79 m/s for λ = 895 nm and $\vec{o} \perp \vec{i}$, i. e. $|\vec{o} - \vec{i}| = \sqrt{2}$. This is sufficient for the measurements presented here. As a result of the calibration curve and Eq. (1), the desired velocity v can be obtained from the measured amplitude ratio q.

The maximum measurement rate of an FM-DGV system is equal to the modulation frequency because at least one period of the modulation frequency is necessary for the amplitude estimation [12]. Here, the modulation frequency is 100 kHz [10]. For achieving such high measurement rates however, a sufficient signal to noise ratio (SNR) is necessary. Otherwise large errors can occur when dividing A_1 by A_2, because of a division by zero or near zero. At the same time, the shorter averaging time associated with high measurement rates lowers the SNR which can only be counteracted by increasing the power of the scattered light. High scattered light powers are obtained for instance by employing a high power laser, high seeding concentrations and using large apertures for light detection. These factors often limit the achievable measurement rate [8,13]. Therefore, a proof-of-principle experiment is inevitable to determine the capabilities of the FM-DGV technique in combination with an imaging fiber bundle for characterizing velocity oscillations in engine inlet flows.

3. Experimental setup

a) Experiment
The inlet model is depicted in Fig. 3a. The flow is induced by sucking the surrounding air. A seeding particle generator with its seeding output was mounted 1.5 m upstream of the inlet entry with minimal disturbance on the intake flow. Measurements were performed at two mass flow rates: 0.5 kg/s and 1 kg/s. The shape of the inlet corresponds to a "bellmouth" inlet, which is a standard shape. The inner diameter of the inlet model amounts to 107.4 mm. A so-called distortion plate can be mounted in the middle of the inlet (see Fig. 3b), which introduces turbulence and is typically used for calibrating the inlet flow measurement. Measurements were performed with and without distortion plate.
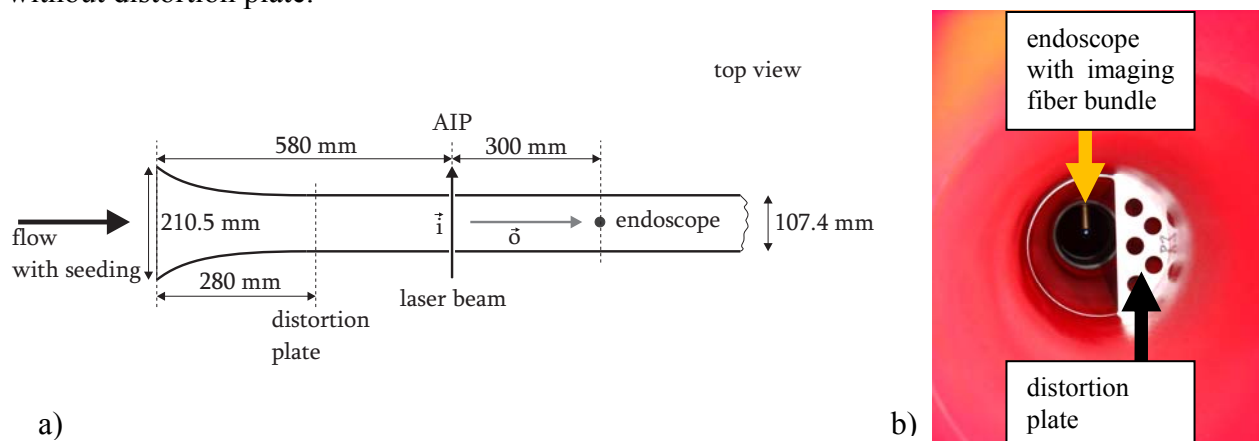

Fig. 3 a) Sketch of the inlet model and b) photo of the view downstream into the inlet showing the mounted distortion plate typically used for calibration. The probe head of the imaging fiber bundle for the scattered light detection is visible in the background.

All measurements take place in the aerodynamic interface plane (AIP), which is located 580 mm from the inlet entry. In order to be able to illuminate the flow in the AIP, a 2 mm wide gap exists here covered by glass windows. Since a gap exists on both sides of the tube, the laser light can pass the cross-section of the tube to avoid reflections.

The scattered light is observed via an endoscope probe that is mounted at the tube center 300 mm downstream of the measurement plane. The rather long distance from the AIP was chosen to avoid upstream flow disturbances by the endoscope probe. The endoscope is connected to an imaging fiber bundle of 4.5 m length. The endoscope optics images the AIP onto the fiber bundle, which consists of 420 x 420 individual fibers at 10 μm pitch. The number of elements limits the effective spatial resolution of the AIP to about 250 μm.

Using a fiber coupled laser for illumination as well, the FM-DGV measurement system was applied by an all-fiber based connection. As a result of this flexible attachment, the measurement equipment could be located in the neighboring from where it was operated. A photo of the experiment is shown in Fig. 4a.
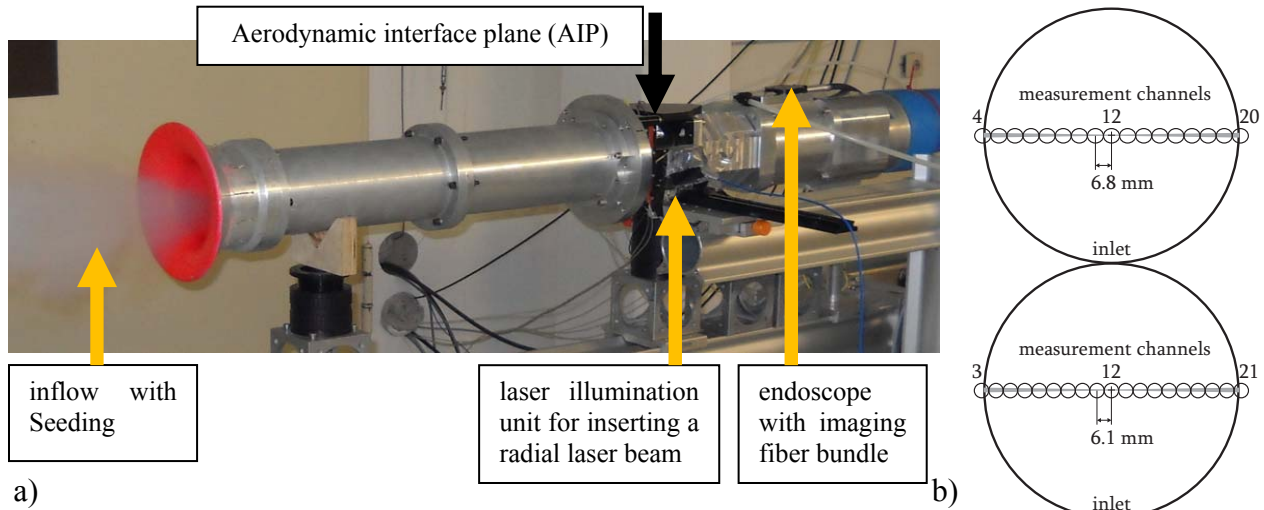

Fig. 4 a) Experimental setup at the inlet test rig and b) arrangement of the array measurement points when operating with low (bottom) and high (top) effective numerical aperture (view from inlet entry).

It is important to note, that particle image velocimetry (PIV) is difficult to apply here. Due to the low spatial resolution of the imaging fiber bundle (250 μm in physical space), the interrogation window size (typically 16x16 pixel – 32x32 pixel) would limit the effective spatial resolution to about 4 mm [14]. Furthermore, the scattered light intensity of a single particle imaged through the fiber bundle will be low and the axial (out-of-plane) velocity component cannot be resolved with the present illumination concept. Consequently, DGV techniques are more appropriate for this application allowing higher spatial resolution, higher scattered light intensities by evaluating cumulative intensity from multiple particles and resolution of the out-of-plane velocity component.

b) Measurement system
The applied FM-DGV measurement system was optimized for achieving a high signal-to-noise ratio to allow high measurement rates. First of all, a high power laser system from the company Toptica Photonics was selected consisting of a master-oscillator-power-amplifier setup. The laser allows fast frequency modulation with 100 kHz, has narrow band width, whose wavelength is compatible with a molecular resonance and includes a fiber coupling. The master oscillator is a diode laser operating at 895 nm wavelength (corresponding to an atomic resonance of cesium gas [11]) and ensuring low bandwidth < 1 MHz and fast frequency modulation capability. In addition, a fiber coupling dock exists for coupling the laser light into a single-mode fiber. The measured power in the measurement volume was about 0.4 W. In order to maximize the available laser power per measurement point, a radial line in the AIP was illuminated with a circular laser beam and the array measurement points were aligned linearly along this line. The laser beam was achieved by focusing the fiber output with a single lens (cf. Fig. 4, illumination unit). This yielded a beam diameter of 2 mm at the tube wall and a waist of 0.5 mm at the tube center.

The scattered light was observed via the imaging fiber bundle by the FM-DGV receiving unit described in [8]. The image of the illuminated line in the AIP on the fiber bundle exit was imaged through a molecular absorption cell filled with cesium gas onto 24 multimode fibers in a linear arrangement each connected with an avalanche photo diode. According to the optical magnification, the distance between two measurement points was about 6.1mm. The lateral extent (spatial resolution) of one measurement point is of similar size. The low spatial resolution allows achieving a high SNR by collecting the scattered light from a multitude of seeding particles. Further experiments were performed with an improved effective numerical aperture (factor 2.4) leading to 6.8 mm point-to-point distance. Hence, 18 or 16 measurement points were equally distributed over the radial line in the AIP as shown in Fig. 4b.

In order to supply high seeding concentrations for achieving high signal to noise ratios, a smoke generator based on an evaporation-recondensation principle of mineral oil was used (Model ViCount 5000). According to the data sheet the average particle diameter is about 200 nm – 300 nm. A centrifuge filter upstream of the delivery point removed larger droplets in the micrometer range. For the average particle diameter 250 nm, the particle response time is 208 ns, which yields a maximum slip of only 0.002 % up to oscillation frequency of 5 kHz [15]. Thus, the slip is negligible small. The seeding particle concentration is not exactly known. However, the average oil consumption was about 1.5 l/h.

Further details about the FM-DGV measurement system can be found in [10-13]. The calibration curve is shown in Fig. 2. According to the FM-DGV measurement principle and the employed setup, one velocity component is measured along a radial line in the AIP. A single component measurement is sufficient for a first proof-of-principle experiment, because the flow direction without distortion plate is known to be axially symmetric. Since the sensitivity direction is 45° off the observation direction $\vec{o}$ (see Fig. 3a), the measured velocity component has to be multiplied by $\sqrt{2}$ to obtain the axial inlet flow velocity.

4. Measurement results

Mean scattered light power as a measure of the signal to noise ratio
In order to characterize the measurement results regarding the achievable measurement uncertainty, the mean detected scattered light power is evaluated first as a measure of the signal-to-noise ratio. Measurement data obtained without the presence of the distortion plate are shown in Fig. 5a and Fig. 5b for 0.5 kg/s and 1 kg/s, respectively. In addition, the mean scattered light power is shown with respect to the radial tube position for the first configuration of the receiving optics having a lower effective numerical aperture (NA) and the second configuration with a higher effective numerical aperture. Obviously, the detected scattered light power was increased by increasing the effective numerical aperture. For instance, at 1 kg/s, the maximum scattered light power was increased from 0.11 nW to 0.36 nW. However, the scattered light powers at the tube boundary are in general lower than at the tube center, especially for 1 kg/s operating with lower effective NA. This is a result of an inhomogeneous seeding particle concentration, which was counteracted during the measurements with the higher NA by a more global seeding at the inlet entry. Similar aspects can be found in the FM-DGV measurement results with distortion plate. The corresponding scattered light powers are shown in Fig. 6a and Fig. 6b. The occasionally high values at the left boundary are likely to be caused by reflections of the laser beam at the tube housing as a result of vibrations on the light supply fixture.
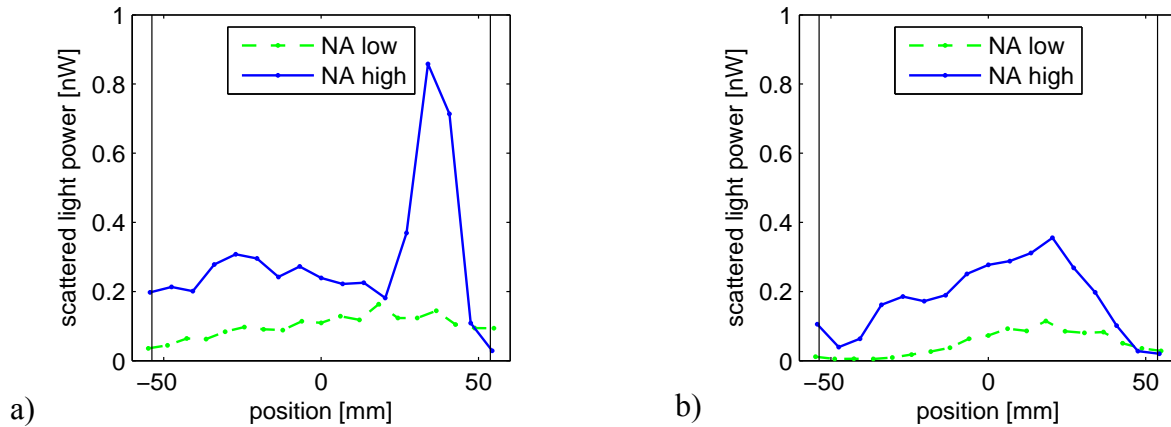
Fig. 5 Measurement without distortion plate: Scattered light powers at a) 0.5 kg/s and b) 1 kg/s air mass flow rate.
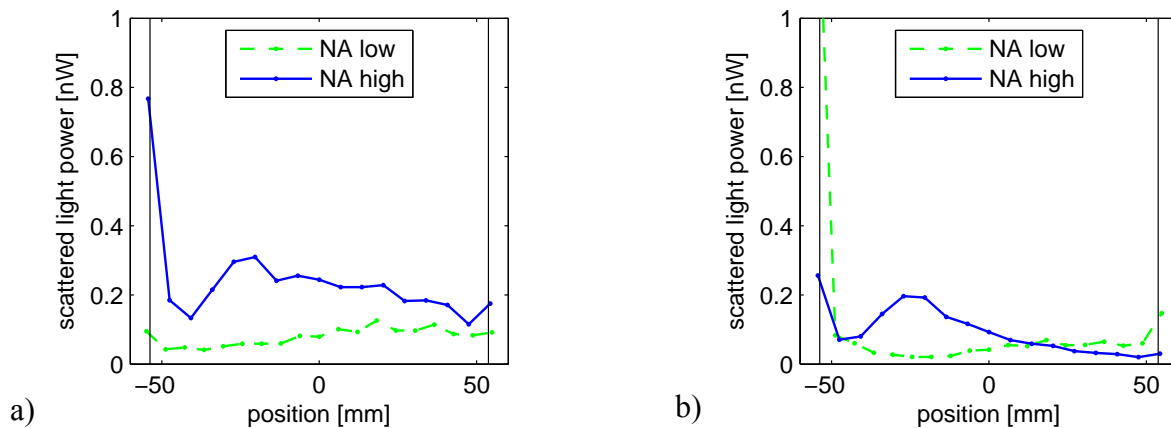

Fig. 6 Measurement with distortion plate: Scattered light powers at a) 0.5 kg/s and b) 1 kg/s air mass flow rate.

The evaluation of the scattered light powers shows, that mean scattered light powers of 0.3 nW are feasible. According to the error estimation given in [9], the resulting minimum achievable velocity standard deviation amounts to $0.03 \text{ m/s} / \sqrt{T/s}$ with T as temporal resolution.

Mean velocity profiles
In order to validate the measurement results, the mean velocity profiles are considered first. Here, 10000 subsequent measurements with a measurement rate of 10 kHz were acquired. To avoid division by zero or near zero (see section 2), a threshold of 0.05 nW was used to discard velocity values resulting from a low scattered light power. The obtained mean velocity profiles without the presence of the distortion plate are shown in Fig. 7a and Fig. 7b and exhibit 95 % confidence levels for 0.5 kg/s and 1 kg/s air mass flow rates, respectively. The velocity profile at 0.5 kg/s shows the expected top-hat shape. The velocity decreases at the boundary regions. However, it does not reach zero, because the average velocity over the entire measurement volume of one channel is measured, which is never zero. At 1 kg/s, the measurement with the lower effective NA obviously contains large systematic errors, while the expected top-hat shape of the velocity profile is obtained when measuring with the higher effective NA. With the higher effective NA for instance, the standard deviation of the mean velocity is minimum at the flow center and amounts to 0.05 m/s and 0.09 m/s at 0.5 kg/s and 1 kg/s, respectively. This is close to the estimated value of 0.03 m/s. The remaining deviation is due to flow turbulence not taken into account in the estimation.

For validation purposes, the measured average velocities at the center (-30 mm to +30 mm) are considered amounting to 47.3 m/s and 91.0 m/s, respectively. They are larger than the theoretical

values, which are derived from the measured air mass flow rate and the assumption of a rectangular shaped velocity profile: 46.0 m/s and 90.1 m/s. This is in excellent agreement with theory, because the velocity must decrease near the walls. However, the measured velocity profiles (for high effective NA) correspond to air mass flow rates of 0.48 kg/s and 0.83 kg/s, respectively, neglecting air compressibility and using the air density 1.2 kg/m^3 (18 °C, 100320 Pa). These mass rates are 4 % and 15 % smaller than the air mass flow rates provided by the Venturi measurement system further downstream of the inlet test section (0.50 kg/s and 0.98 kg/s). For the high mass flow rate, the velocities measured at the near-wall channels are probably underestimated by a low signal to noise ratio. If increasing the threshold to 0.1 nW for instance, the remaining deviation of the mass rate is only -6 % at 0.98 kg/s. Furthermore, light reflections at the wall might occur which also lowers the measured velocity values at the near-wall channels, which has to be calibrated. Additional factors that need to be considered are the compressibility of air as well as the need for on-site calibration of the FM-DGV system. In the present case, the calibration was performed in the laboratory in Dresden several days before the measurements in Cologne. In spite of these issues, the qualitative validation of the measurement system was already successful.
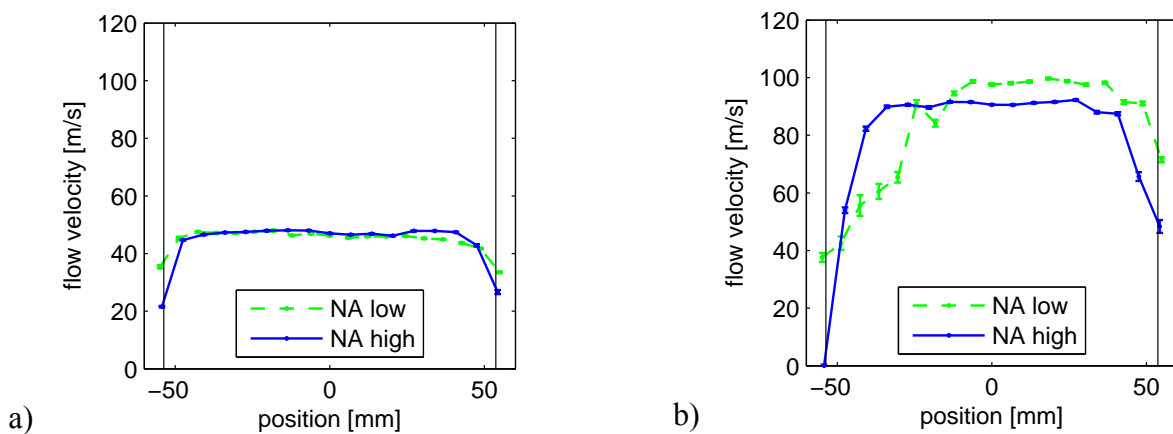

Fig. 7 Measurement without distortion plate: mean velocity profiles at a) 0.5 kg/s and b) 1 kg/s air mass flow rate with 95 % confidence levels.
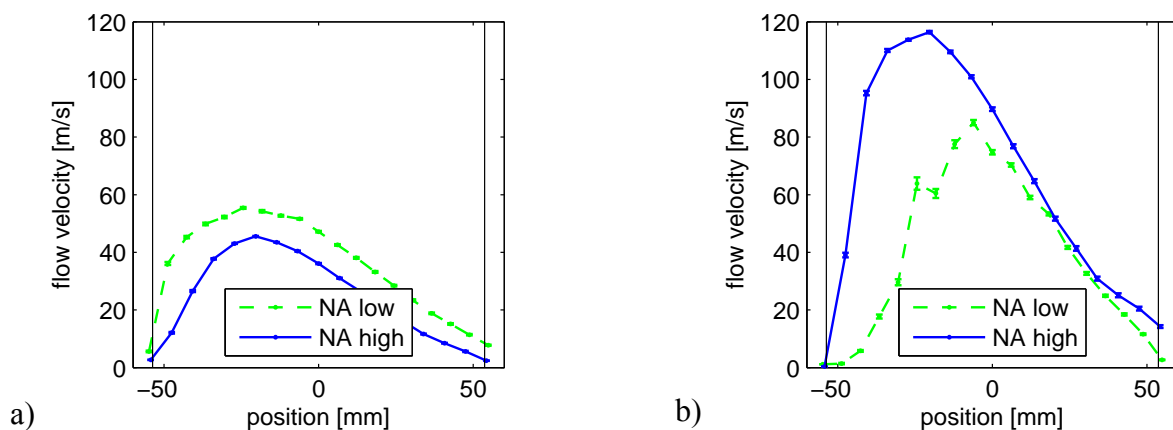

Fig. 8 Measurement with distortion plate: mean velocity profiles at a) 0.5 kg/s and b) 1 kg/s air mass flow rate with 95 % confidence levels.

The corresponding mean velocity profiles downstream of the distortion plate are shown in Fig. 8a and Fig. 8b. Since the flow is no longer axially symmetric, the actually measured velocity component was considered (see section 3). It is maximum in the center of the left part of the tube und decreases almost linearly at the right part of the tube. Large deviations occur between the low NA and high NA configuration. The assumed reason of it is the low signal to noise ratio for the low NA measurement, which has to be analyzed further.

Effective measurement rate

A key question of this feasibility study is whether FM-DGV is capable of achieving high measurement rates when using an imaging fiber bundle and an endoscope. In order to answer this question, the number of validated velocity samples (using a threshold at 0.05 nW scattered light power) out of 10000 subsequently measured samples is shown in Fig. 9 (no distortion plate) and Fig. 10 (with distortion plate). Without going into detail here, measurement rates up to 8 kHz and higher could be achieved. For this purpose, a dense and homogeneous seeding is crucial, which is illustrated by two examples: Lower measurement rates occur e. g. in Fig. 9b (no distortion plate, 1 kg/s) at the boundary, because the seeding requirements were difficult to achieve there. Considering Fig. 9a (no distortion plate, 0.5 kg/s), the number of valid samples in the tube center region does not increase when measuring with a higher NA, although the mean scattered light power was increased (cf. Fig. 5a). Obviously, a dense seeding was not continuously available. Nevertheless, the FM-DGV technique was proven to be in general capable of achieving the desired measurement rate ≥ 4 kHz in an inlet flow.
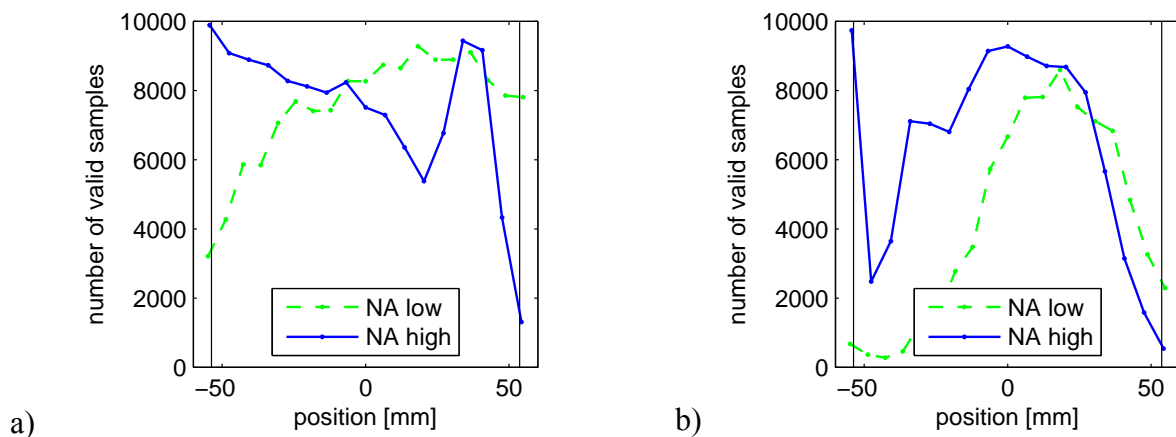
a) b)

Fig. 9 Measurement without distortion plate: Number of valid velocity samples at a measurement duration of 1 s with 10 kHz measurement rate at a) 0.5 kg/s and b) 1 kg/s air mass flow rate.
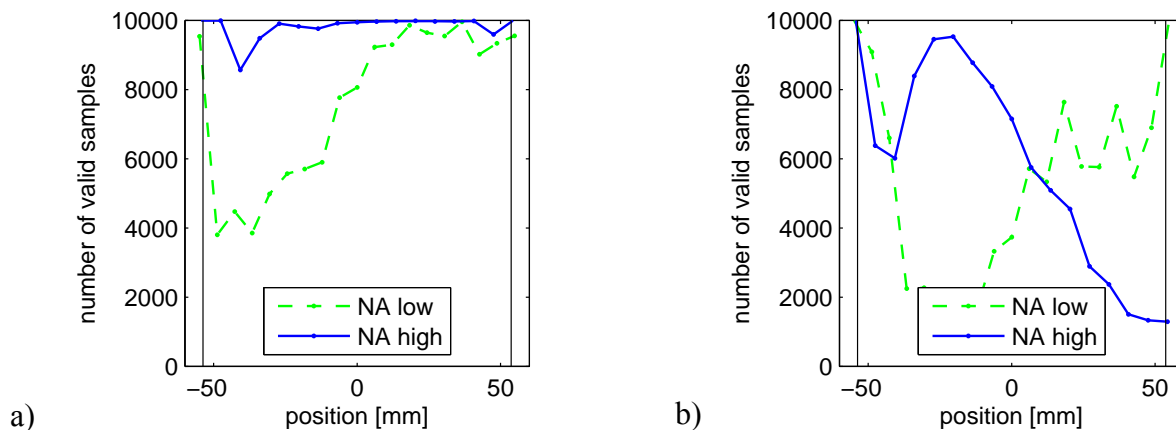
a) b)

Fig. 10 Measurement with distortion plate: Number of valid velocity samples at a measurement duration of 1 s with 10 kHz measurement rate at a) 0.5 kg/s and b) 1 kg/s air mass flow rate.

Velocity spectra

Finally, the velocity spectra were evaluated for characterizing the inlet flow. The invalid samples were substituted by estimated values using linear interpolation between the neighboring values [16]. For each experiment, 10 sequences of 1s duration were acquired at a sampling rate of 10 kHz. The (two-sided) power spectral density (PSD) of the velocity was calculated using a fast Fourier transform over each 1 s long measurement. This yields a frequency resolution of 1 Hz. Finally, the ten PSDs were averaged. To improve the visualization, a moving average filter over 10 Hz was also applied.

Only the measurement results with the higher effective NA are presented. For comparing the PSD with and without distortion plate, the actually measurement velocity component is considered here. The PSD of channel 17 (radial position 33.9 mm) is shown for 0.5 kg/s and 1 kg/s in Fig. 11a (no distortion plate) and Fig. 11b (with distortion plate), respectively. Flow oscillations up to about 1 kHz were resolved. The PSD decreases monotone with frequency and has no resonance peaks. The PSDs for 0.5 kg/s are smaller than the PSDs for 1 kg/s. Indeed, the PSDs are similar when scaling the frequency axis accordingly, which is as expected.
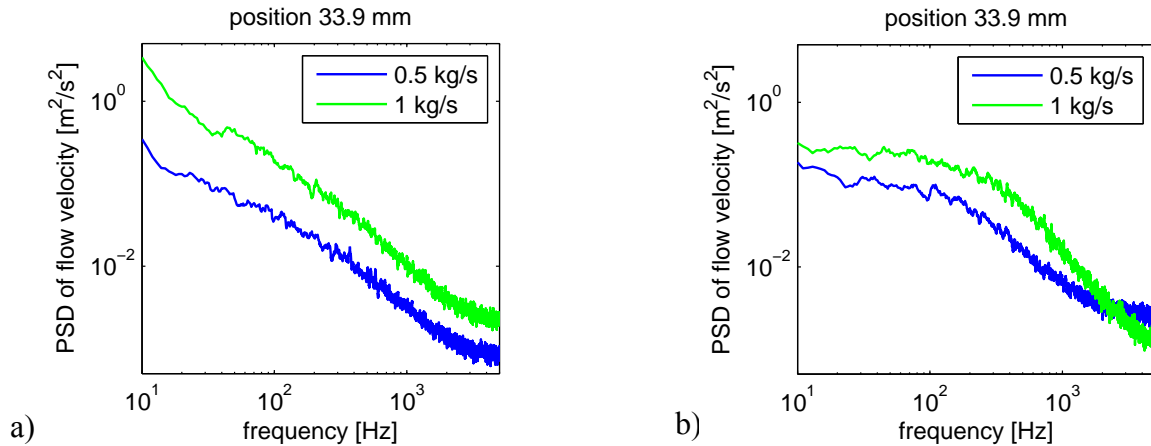
Fig. 11 Power spectral density of the measured velocity from channel 17 (radial position 33.9 mm) for 0.5 kg/s and 1 kg/s air mass flow in case of a) no distortion plate and b) inserted distortion plate.

Comparing the PSDs for no distortion plate and with distortion plate for channel 17 (radial position 33.9 mm) at the right part of the tube (see Fig. 12a and Fig. 12b), the PSD increases when the distortion plate is present. However, the PSD for no distortion plate is larger for frequencies below 30 Hz and 100 Hz, respectively. The distortion plate is assumed to damp these large scale vortices, which is in agreement with turbulence theory. Similar results are also visible for channel 8 at the left part of the tube (radial position -27.1 mm), which are shown in Fig. 13a and 13b. The distortion plate causes oscillations with larger amplitudes than at the right part of the tube. This non-symmetric behavior is due to the asymmetric shape of the distortion plate (see Fig. 3b). As a result, the inlet flow and its disturbance by a distortion plate were successfully characterized by FM-DGV measuring flow velocity spectra.
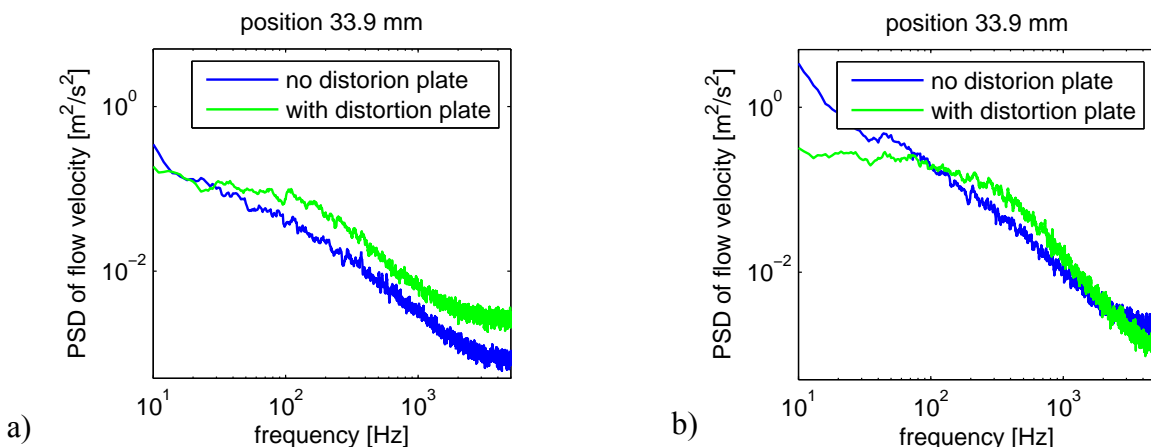
Fig. 12 Power spectral density of the measured velocity from channel 17 (radial position 33.9 mm) comparing the effect of the distortion plate for a) 0.5 kg/s and b) 1 kg/s air mass flow.
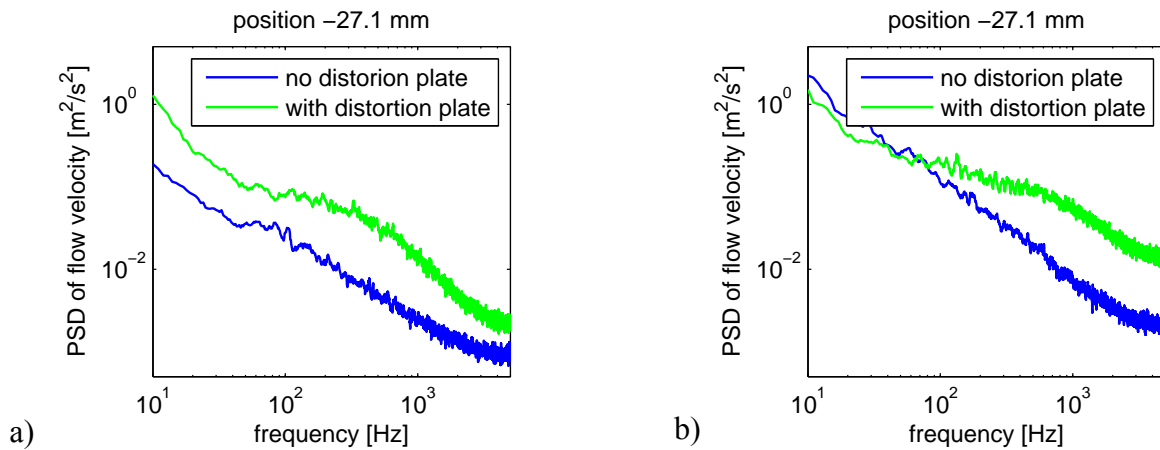
Fig. 13 Power spectral density of the measured velocity at channel 8 (radial position -27.1 mm) comparing the effect of the distortion plate for a) 0.5 kg/s and b) 1 kg/s air mass flow.

5. Outlook

The experiment investigated the potential of FM-DGV when used with an imaging fiber bundle and an endoscope for characterizing inlet flows. The investigation showed, that the performance can be improved further by several factors. The key issue is to achieve a sufficiently high signal to noise ratio, which can be increased for instance by increasing the laser power using an additional power amplifier or improving the fiber coupling efficiency by using a multi-mode fiber. Another option is to use larger seeding particles to increase the scattering cross section. As an example, common particles made of Di-ethyl-hexyl-sebacat with 1 μm in diameter can be used (response time 3.4 μs, slip 0.6 %@5 kHz) [15]. In addition, the effective numerical aperture can also be increased by using absorption cells with larger diameters. Finally, the mechanical stability of the laser light supply can be improved avoiding disturbing reflections at the tube walls for the near wall measurements.

6. Conclusion

The FM-DGV measurement technique was successfully applied for the first time with an imaging fiber bundle and an endoscope for characterizing non-intrusively an inlet flow. The proof-of-principle experiment was performed on an inlet model with 107.4 mm in diameter in the aerodynamic interface plane (AIP) having an air mass flow of 0.5 kg/s and 1 kg/s, respectively. The array measurement points were aligned at a radial line in the AIP providing 16 points. As a result, more measurement points were available at this line than with the standard procedure (10 pressure probes per line). However, the key challenge was to increase the measurement rate beyond 4 kHz in order to obtain unsteady velocity data. In the experiment, measurement rates up to 8 kHz were achieved. Hence, FM-DGV meets the principle requirements for characterizing inlet flows.

Mean velocity profiles and power spectral density of the velocity were measured for an unobstructed inlet and an inlet with a distortion plate. The mean velocity profiles were validated by the given air mass flow rates. The spectra show velocity oscillations up to about 1 kHz and, as expected, stronger oscillations when the distortion plate was inserted. Below 100 Hz, the oscillations were damped depending on the radial position. For these reasons and because of the numerous improvement possibilities mentioned in the outlook above, the FM-DGV technique is considered to be a promising approach for the non-intrusive characterization of inlets for aircraft engines. Hence, the measurement of multiple components and multiple radial lines has to be considered next.

Acknowledgement

References

[1] N. C. Bissinger, T. Breuer: "Basic Principles – Gas Turbine Compativility – Intake Aerodynamic Aspects", *Encyclopedia of Aerospace Engineering*, Vol. 8, Chapter EAE487, John Wiley&Sons, 2010.

[2] W. T. Cousins: "History, philosophy, physics, and future directions of aircraft propulsion system / inlet integration", *ASME Turbo Expo 2004*, Paper GT2004-54210 (16pp), Vienna, 2004.

[3] I. Roehle, C. Willert, R. Schodl: "Recent applications of three-dimensional Doppler global velocimetry in turbo-machinery", 9th *Int. Symp. on Applications of Laser Techniques to Fluid Mechanics*, Paper 34-2 (8pp), Lisbon, 1998.

[4] C. Willert, G. Stockhausen, J. Klinner, C Lempereur, P. Barricau, P. Loiret, J. C. Raynal: "Performance and accuracy investigations of two Doppler global velocimetry systems applied in parallel", *Meas. Sci. Techn.* 18: 2504–2512 2007.

[5] D. S. Nobes, H. D. Ford, R. P. Tatam: "Instantaneous, three-component planar Doppler velocimetry using imaging fibre bundles", *Exp. in Fluids* 36:3-10, 2004.

[6] C. Willert, G. Stockhausen, M. Beversdorff, J. Klinner, C. Lempereur, P. Barricau, J. Quest, U. Jansen: "Application of Doppler global velocimetry in cryogenic wind tunnels", *Exp. in Fluids* 39: 420–430, 2005.

[7] U. Dierksheide, P. Meyer, T. Hovestadt, W. Hentschel: "Endoscopic 2D particle image velocimetry (PIV) flow field measurements in IC engines", *Exp. in Fluids* 33: 794-800, 2002.

[8] A. Fischer, L. Büttner, J. Czarske, M. Eggert, H. Müller: "Measurements of velocity spectra using time-resolving Doppler global velocimetry with laser frequency modulation and a detector array", *Exp. in Fluids* 47: 599 – 611, 2009.

[9] A. Fischer, L. Büttner, J. Czarske, M. Gottschall, R. Mailach, K. Vogeler: "Investigation of the Tip Clearance Flow in a Compressor Cascade Using a Novel Laser Measurement Technique with High Temporal Resolution", *Journal of Turbomachinery* 134:051004 (9 pp.), 2012.

[10] A. Fischer, L. Büttner, J. Czarske, M. Eggert, G. Grosche, H. Müller: "Investigation of time-resolved single detector Doppler global velocimetry using sinusoidal laser frequency modulation", *Meas. Sci. Tech.* 18: 2529 – 2545, 2007.

[11] A. Fischer, L. Büttner, J. Czarske: „Simultaneous measurements of multiple flow velocity components using frequency modulated lasers and a single molecular absorption cell", *Optics Communications* 284: 3060-3064, 2011.

[12] A. Fischer, L. Büttner, J. Czarske, M. Eggert, H. Müller: "Array Doppler Global Velocimeter with Laser Frequency Modulation for Turbulent Flow Analysis – Sensor investigation and application", in: *Imaging Measurement Methods for Flow Analysis* (Eds. W. Nitsche, C. Dobriloff), Springer, Berlin, p. 31-41, 2009.

[13] A. Fischer, J. König, J. Czarske: "Speckle noise influence on measuring turbulence spectra using time-resolved Doppler global velocimetry with laser frequency modulation", *Meas. Sci. Tech.* 19: 125402 (15 p.), 2008.

[14] J. Westerweel: "Fundamentals of digital particle image velocimetry", *Meas. Sci. Tech.* 8: 1379-1392, 1997.

[15] H.-E. Albrecht, M. Borys, N. Damaschke, C. Tropea: "Laser Doppler and Phase Doppler Measurement Techniques", Springer, Berlin, 2003.

[16] A. Ramond, P. Millan: "Measurements and treatment of LDA signals, comparison with hot-wire signals", *Exp. in Fluids* 28: 58-63, 2000.